Z. Phys. A 350, 101–113 (1994)

ZEITSCHRIFT
FÜR PHYSIK A

Subthreshold antiproton and K^- production in heavy ion collisions

A. Schröter[1], **E. Berdermann**[1], **H. Geissel**[1], **A. Gillitzer**[2], **J. Homolka**[2], **P. Kienle**[2], **W. Koenig**[1], **B. Povh**[3], **F. Schumacher**[2], **H. Ströher**[4]

[1] Gesellschaft für Schwerionenforschung, D-64220 Darmstadt, Germany
[2] Technische Universität München, D-85748 Garching, Germany
[3] Max-Planck-Institut für Kernphysik, D-69029 Heidelberg, Germany
[4] Universität Gießen, D-35392 Gießen, Germany

Received: 3 February 1994 / Revised version: 31 May 1994

Abstract. Subthreshold $\bar{p}$ and K^- and energetic π^- production was studied in Ne+NaF, Cu, Sn and Bi, and in Ni+Ni collisions with incident energies between 1.6 and 2 GeV/u. The measured cross sections indicate a dominant contribution of baryonic resonances. This is also consistent with a generalized scaling behaviour of the cross sections with the energy available in the collision and the energy necessary to produce particles as observed with Ne induced reactions. Deviations from scaling especially pronounced in the Ni−Ni system will be discussed in terms of absorption effects. The flat slope of the excitation function for $\bar{p}$ production can be related to a reduced production threshold caused by a reduction of the antiproton mass in the dense and heated medium by about 100–150 MeV/c^2. A similar in-medium mass reduction is also indicated for K^- mesons. An increased $\bar{p}$ reabsorption probability for the heavier systems is concluded from the comparison of the $\bar{p}$ yields in Ne+NaF, Ne+Sn and Ni+Ni collisions.

PACS: 25.70.Np

1. Introduction

The properties of nuclear matter under extreme conditions, which may exist in astrophysical scenarios such as supernovae and neutron stars, can be studied in the laboratory only in relativistic heavy ion collisions. At incident energies of ~2 GeV/u for a short time interval of 10–20 fm/c nuclear matter is compressed up to about 3 times the normal nuclear matter density ρ_0 and heated to temperatures of ~100 MeV. Information on the behaviour of nuclear matter under such conditions may be obtained either by analysing the particle flow in the nuclear disassembly or by studying secondary particles produced in the collision. If these particles are such massive or energetic that they cannot be produced in nucleon-nucleon collisions at the given center of mass energy, they are created in multistep processes and preferentially in an early stage of the collision at high density. The mechanism of subthreshold particle production and the sensitivity of different particle species to the macroscopic properties of nuclear matter has been discussed in comprehensive reports or reviews [1, 2].

Among all studied secondary particles, antiprotons have the highest threshold energy of 5.6 GeV for creation in a nucleon-nucleon collision. Nevertheless this extreme subthreshold process has been observed at the BEVALAC [3] in 2 GeV/u and 1.65 GeV/u ^{28}Si+Si and 2 GeV/u ^{20}Ne+NaF reactions, and at considerably higher energies at the JINR in Dubna [4] in 3.65 GeV/u ^{12}C+Cu collisions.

Shor et al. [5] investigated the measured $\bar{p}$ production cross sections in proton-nucleus and nucleus-nucleus collisions in the framework of a first collision model taking account of the internal momenta of projectile and target nucleons. They considered also a high momentum component of the momentum distribution, adjusted to backward proton emission data. While $p+A\rightarrow\bar{p}+X$ data [6] can be quite well reproduced, the model completely fails for $A+A\rightarrow\bar{p}+X$, giving cross sections by more than three orders of magnitude too low. The effect of multinucleon interactions on the $\bar{p}$ production yield has been analysed by Danielewicz [7]. While the above models assume that the $\bar{p}$ production takes place at the beginning of the collision far from thermal equilibrium, Koch and Dover [8] in a contrary approach examine the contribution of ΔN and $\Delta\Delta$ collisions to the $\bar{p}$ yield in a fireball scenario with thermal and hadrochemical equilibrium. Ko et al. [9], also within the framework of a thermal model, emphasize the role of meson-meson collisions for the $\bar{p}$ production, and find a major contribution from the $\rho\rho\rightarrow p\bar{p}$ channel. With these models only equilibrium $\bar{p}$ abundancies in infinite nuclear matter are obtained and a direct comparison to measured cross sections is not possible. Transport theories like BUU and QMD, taking into account the full dynamics of an heavy ion collision, however in-

Dedicated to Professor Klaus Dietrich on the occasion of his 60th birthday

dicate that the collision time is too short to reach thermal equilibrium [10]. Recently, the transport models have also been used to predict such extreme subthreshold processes as antiproton production [11, 12]. These calculations clearly indicate that multistep processes involving to a large extent Δ and N^* resonances dominate the creation of $p\bar{p}$ pairs. However no quantitative agreement with the experimental data is obtained in these first transport theoretical attempts, since the predicted $\bar{p}$ yield would be still too low if the annihilation of antiprotons were taken into account [11].

Due to their higher mass the Δ and N^* resonances play the role of an energy storage reducing the required amount of kinetic energy for the $\bar{p}$ production. With recent RBUU calculations [13] the result is obtained that at 2 GeV/u incident energy the main contribution to the $\bar{p}$ yield is due to resonance-resonance collisions.

Compared to less absorptive probes like K^+ mesons the experimentally observed $\bar{p}$ yield is more difficult to interpret, since the dominant fraction of the initially produced antiprotons is reabsorbed in the nuclear medium due to the large annihilation cross section. Thus systematic studies of the dependence of the $\bar{p}$ production cross section on the incident energy, the $\bar{p}$ momentum, and the system size are needed in order to disentangle the variation of the primordial production yield and of the reabsorption effects. On the other hand with antiprotons a subthreshold process may be investigated at higher collision energies than with any other secondary particle species studied so far, thus probing highly compressed hadronic matter containing a considerable fraction (up to 30%) of baryonic resonances. At incident energies of $\sim$2 GeV/u $\bar{p}$ production is even below the threshold in a nucleon-nucleon collision, if the Fermi momenta of the target and the projectile nucleons are added to the relative motion. As compared to other probes like K^+ or η mesons [14, 15], the production cross section for antiprotons is therefore much more sensitive to additional processes in the nuclear medium which reduce the effective energy threshold. The Fermi momentum corrected threshold for various secondary particles is shown in Fig. 1.

Since the secondary particle yield at far subthreshold energies is extremely influenced by a shift of the threshold energy, the measured $\bar{p}$ yield is closely connected to the effective antibaryon mass inside the nuclear medium. This is a complementary approach to study the nuclear potential for antibaryons compared to low energetic $\bar{p}$-nucleus scattering [16, 17], where only the outer region of the nucleus with $\rho \ll \rho_0$ is probed due to the large annihilation probability.

In Sect. 2 the experimental method is discussed and in Sect. 3 the experimental results are presented. Section 4 summarizes the discussion under various subsections. Subsection 4.1 addresses the enhancement of antiproton production in nucleus-nucleus collisions. The observed scaling pattern of the particle production over a wide range of production energies is discussed in Subsect. 4.2. In Subsect. 4.3 the excitation function for $\bar{p}$ production is compared to the incident energy dependence of K^- and π^- production. In the following Subsect. 4.4 the dependence of the $\bar{p}$ production cross sections on the system size is interpreted in comparison to the predictions of a simple geometrical fireball model. As the A dependence, also the momentum dependence of the $\bar{p}$ yield discussed in Subsect. 4.5 will be considerably influenced by the reabsorption probability. The magnitude and the energy dependence of the $\bar{p}$ production cross sections are compared to the results of recent transport models in Subsect. 4.6.

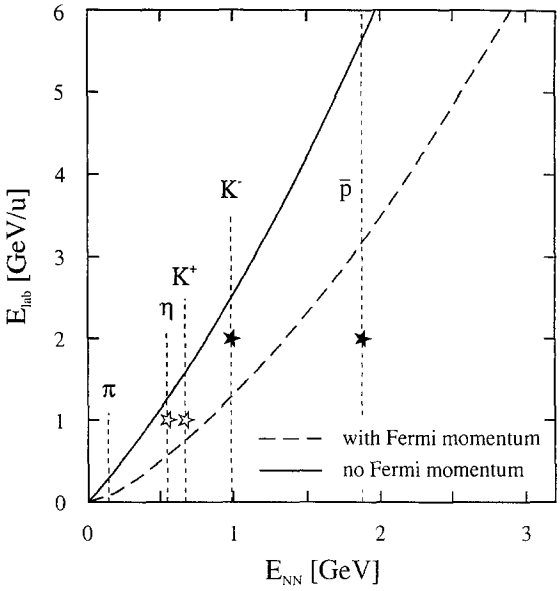

Fig. 1. Contribution of the Fermi momentum to the threshold energy for the production of various secondary particles. The *dashed line* shows the threshold energy in the lab system as a function of the c.m. energy in the collision of two nucleons for a maximum contribution of their internal momenta with $p_F = 260$ MeV/c. The *asterisks* demonstrate the extreme subthreshold character of the $\bar{p}$ production at 2 GeV/u compared to the production of K^- at 2 GeV/u (this work) or e.g. of K^+ [14] or η [15] at 1 GeV/u

2. Experimental method

At bombarding energies in the range of 2 GeV/u, the $\bar{p}$ and K^- production cross section is very small, while pions are abundantly produced. Therefore a very efficient and unambiguous particle identification is required.

Ion beams extracted from the synchrotron SIS at GSI are focussed on targets with a thickness corresponding to about 30% of the interaction length. Negatively charged particles emitted from the target at 0° are selected by the Fragment Separator FRS [18], a magnetic 0° spectrometer of 72 m length with 4 dipole magnets and 4 focal planes ($S1 - S4$). Since high momentum resolution is not required, a special "high acceptance" mode, which is non-dispersive at each of the focal planes, was developed [19], in order to increase the rate of observable antiprotons. A solid angle of 3 msr and a momentum acceptance $\Delta p/p = \pm 3\%$ was achieved, ten times more than with the usual setting optimized for momentum resolution. The primary beam and all nuclear fragments are bent off the beamline by the first dipole magnet and do not produce any background from the 2nd to the 4th focal

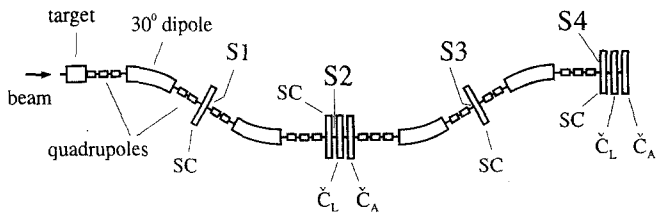

SC : scintillation detector
$\check{C}_L$: lucite Čerenkov detector
$\check{C}_A$: aerogel Čerekov detector
S1...S4 : focal planes of the separator

Fig. 2. Schematic view of the experimental set-up. The total length of the spectrometer is 72 m. The target chamber and the detectors are not drawn in correct scale

plane. The intensity ratio of negatively charged particles, however, differs by many orders of magnitude, e.g. at a momentum of 1.5 GeV/c the intensity ratio is roughly $N_{\pi^-}:N_{K^-}:N_{\bar{p}} \approx 10^7:3000:1$. For pion discrimination the times of flight and the velocities of the particles are therefore determined several times independently. At each of the focal planes a time signal is taken from horizontally placed position sensitive plastic scintillators, yielding the times of flight for 3 sections of the separator ($S1-S2$, $S2-S3$, and $S3-S4$). In addition, both at the central and the final focal planes ($S2$ and $S4$) two Čerenkov detectors with different thresholds (lucite and aerogel) were used in a veto mode to distinguish the different particle species. A schematic view of the set-up is shown in Fig. 2. The lucite detectors in total reflection geometry with a velocity threshold $\beta_{thr}=0.90$ veto pions of all momenta in the relevant momentum range and K^- with $p>1$ GeV/c. In order to be sensitive for the K^-, the aerogel Čerenkov detectors with a threshold $\beta_{thr}=0.96$ are used, vetoing kaons only at momenta above 1.7 GeV/c. The event trigger was generated by one of the following conditions: a signal from the $S2$ scintillator and no veto signal from the $S2$ aerogel Čerenkov detector, a signal from the $S4$ scintillator and no veto signal from the $S4$ lucite Čerenkov counter, a coincidence of a combination of scintillator signals ($S1$ and $S2$, or $S2$ and $S4$) matching the $\bar{p}$ time of flight, or one of the single events from any of the scintillators at a strongly downscaled rate. The latter single triggers were used to measure the pion rate at each of the focal planes, and thereby to control the transmission through the spectrometer. The transmission for π^- and K^- was corrected for the decay of the particles, to obtain the yield at the position of the target. For 1.5 GeV/c momentum, at the central focal plane 66% of the pions and 4.3% of the kaons have survied. At 1.0 GeV/c the fraction is reduced to 53% and 0.9% respectively. From the variation of the ratios of the π^- rates at the different focal planes we conclude that the transmission through the spectrometer varied by less than 10% during the experiment.

Prior to the $\bar{p}$ and K^- production runs the whole set-up was tested with positively charged particles (α, d, p, π^+) and the setting of the beam optical components was optimized for maximum transmission of protons. This setting differs only slightly from the values for the optimum pion transmission due to the different energy loss of pions and protons in the detectors and the vacuum windows. Good agreement with the predicted values from the Monte Carlo simulation [19] was obtained both for the transmission and for the spatial distribution of the protons at the focal planes ($\Delta x \approx 10$ mm at $S4$).

The beam intensity was monitored by measuring the current of secondary electrons emitted from a set of aluminium foils, which are passed by the beam in front of the target [20]. The beam monitor was calibrated at low intensities $< 10^6$ ions/s, where single counting of projectiles with a scintillator was still possible. The absolute value of the intensity measured in that way is estimated to be correct within 20%. The maximum available beam intensities were $3\cdot10^9$ ^{20}Ne ions/spill and $3\cdot10^8$ ^{58}Ni ions/spill with a spill duration of 2 s and a repetition rate of 0.2 spills/s.

Very good background suppression allowing backgroundfree identification of antiprotons was obtained from the Čerenkov counters at the central focal plane. In Fig. 3 a time of flight spectrum for the FRS segment $S2-S3$ is shown for events which passed the anticoincidence filter of the aerogel Čerenkov detector at $S2$ (upper part) and for events with no veto signal from either of the Čerenkov detectors at $S2$ (lower part). By these

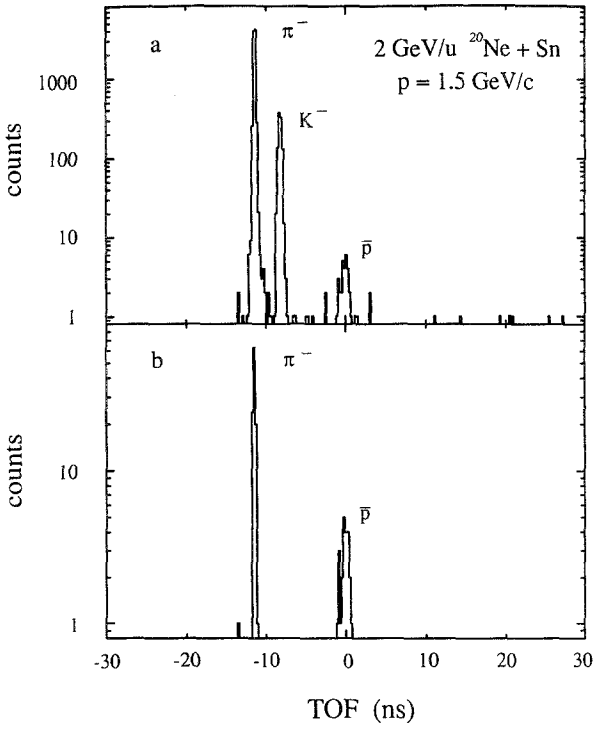

Fig. 3.a, b. Time of flight spectrum of negatively charged particles in the reaction 2 GeV/u ^{20}Ne + Sn at $p=1.5$ GeV/c for the spectrometer segment $S2$–$S3$. In spectrum **a** only events with no signal in the aerogel Čerenkov counter at $S2$ were accumulated, for spectrum **b** in addition the veto filter of the lucite Čerenkov detector was required. The corresponding total amount of pions detected at the focal plane $S3$ was $1.3\cdot10^8$

veto conditions the π^- rate is reduced by more than 4 orders (aerogel) and by more than 6 orders of magnitude (both lucite and aerogel) respectively, i.e. the number of pions not seen by the Čerenkov counters is extremely small. The pulse height distribution of the scintillator signals for the $\bar{p}$ events is in agreement with the pulse height spectrum measured for protons. In addition it was verified that the times of flight for the $\bar{p}$ events are consistent with each other for all FRS segments ($S1-S2$, $S2-S3$, $S3-S4$). However, due to the high efficiency of the veto detectors the last segment of the spectrometer was not required for a background free detection of antiprotons.

In order to extract production cross sections, the measured particle yields were corrected for absorption effects of the projectile ions and of the secondary particles in the target. The obtained production cross sections refer to the mean projectile energies taking into account the energy loss in the target.

3. Experimental results

^{20}Ne beams at incident energies of 2.0, 1.8 and 1.6 GeV/u were focussed on NaF (6 cm), Cu (3 cm), Sn (5 cm) and Bi (4.5 cm) targets. The mean projectile energies in the targets were approximately 100 MeV/u lower than the incident energies, namely 1.93 GeV/u, for the NaF target, 1.90 GeV/u for the Cu target, 1.89 GeV/u for the Sn target and 1.87 GeV/u for the Bi target, respectively. Secondary negative particles were measured at momenta of 1.0 and 1.5 GeV/c. The maximum pion rates were as high as $3 \cdot 10^5$/spill.

In a second experiment Ni targets were bombarded with 1.93 and 1.84 GeV/u ^{58}Ni beams. Targets of different thickness (18 mm and 9 mm) were used in order to check the thickness effect on the particle yield. By using the thin target at 1.93 GeV/u and the thick target at 1.84 GeV/u for the $\bar{p}$ production run, the excitation function was measured with a step of 190 MeV/u with respect to the effective incident energy (1.85 and 1.66 GeV/u, respectively). A much larger momentum range was studied for the pions ($0.5\ \text{GeV/c} \leqq p \leqq 2.8\ \text{GeV/c}$) and also for kaons ($1.0\ \text{GeV/c} \leqq p \leqq 2.2\ \text{GeV/c}$) than in the Ne induced reactions. Antiprotons were measured at momenta of 1.5 and 1.9 GeV/c.

As mentioned in Sect. 2, the measured production cross sections of secondary particles cover 9 orders of magnitude, namely from $Ed^3\sigma/dp^3 \approx 30\ \text{b} \cdot \text{GeV}/(\text{GeV/c})^3$ for π^- with 0.5 GeV/c momentum, produced in 1.89 GeV/u ^{58}Ni + Ni collisions, down to $Ed^3\sigma/dp^3 \approx 20\ \text{nb} \cdot \text{GeV}/(\text{GeV/c})^3$ for $\bar{p}$ with 1.5 GeV/c momentum in 1.66 GeV/u ^{58}Ni + Ni collisions. The $\bar{p}$ rate was typically 1–2 $\bar{p}$/h in the ^{20}Ne induced reactions and

Table 1. Survey of measured invariant particle production cross sections $\left(\sigma \equiv E\frac{d^3\sigma}{dp^3}\right)$. Only statistical errors are given. The error due to a possible variation of the transmission through the separator is less than 10%. The calibration of the beam monitor is estimated to be correct within 20%. Some settings were chosen to measure K^- and π^- or π^- only

Projectile	Target	E_{mean} [GeV/u]	p_{lab} [GeV/c]	$\sigma_{\bar{p}}$ $\left[\frac{\text{nb GeV}}{(\text{GeV/c})^3}\right]$	σ_{K^-} $\left[\frac{\mu\text{b GeV}}{(\text{GeV/c})^3}\right]$	σ_{π^-} $\left[\frac{\text{mb GeV}}{(\text{GeV/c})^3}\right]$
^{20}Ne	NaF	1.93	1.0	68.9 ± 18.5	799 ± 21	3 770
			1.5	45.2 ± 8.4	140 ± 5	423
	Cu	1.90	1.5	82.1 ± 13.0	236 ± 7	555
	Sn	1.89	1.0	88.3 ± 24.4	2550 ± 71	7 650
			1.5	88.3 ± 17.0	321.5 ± 10.3	672
		1.69	1.5	33.1 ± 7.6	123 ± 5	369
		1.49	1.5		32.3 ± 3.6	156
	Bi	1.87	1.5	111 ± 19	395 ± 11	796
^{58}Ni	Ni	1.85	0.5			30 140
			0.8			20 190
			1.0	597^{+1373}_{-495}	3390 ± 366	9 840
			1.5	127 ± 38	592 ± 26	960
			1.9	$53.5^{+24.6}_{-17.7}$	187 ± 7	215
			2.2	157^{+207}_{-102}	55.2 ± 5.0	106
			2.75			18.2
		1.66	1.0		1109 ± 171	6 370
			1.5	$22.6^{+11.1}_{-7.9}$	229 ± 8	517
			1.9	117^{+268}_{-97}	59.8 ± 7.8	96.6
			2.5			18.7
			2.8			5.2

$0.3-0.5$ $\bar{p}$/h in the ^{58}Ni + Ni experiment. The number of detected antiprotons at given beam energy, target and secondary particle momentum was typically 20 to 30 $\bar{p}$ in the Ne + X experiment, and 10 $\bar{p}$ in the Ni + Ni experiment, respectively.

K^- and π^- production cross sections were obtained together with those of the antiprotons. Due to time limitations some of the combinations of the incident energy and the secondary momentum were chosen to measure K^- and π^- mesons only. The measured particle production cross sections for all studied collision systems are summarized in Table 1. The magnitude of the π^-, K^- and $\bar{p}$ production cross sections measured in ^{20}Ne + NaF collisions is in good agreement with the measurement of Shor et al. [3], who studied the same reaction. Among the asymmetric systems we investigated the system Ne + Sn most extensively, by varying both the incident energy and the secondary particle momentum. In the collisions of Ne + Cu the particle production cross sections are 20% to 30% smaller than in the Ne + Sn system at the same incident Ne energy of 2 GeV/u, while those for Ne + Bi are 20% to 30% larger. K^- and π^- production cross sections measured in 1.85 and 1.66 GeV/u Ni + Ni collisions as a function of the particle momentum are shown in Fig. 4.

Antiproton production cross sections are shown explicitly in Fig. 5 for 1.93 GeV/u Ne + NaF, 1.89 GeV/u Ne + Sn and 1.85 GeV/u Ni + Ni collisions, the systems which were studied at different $\bar{p}$ momenta. Compared to the momentum dependence of the π^- and the K^- yield, the variation of $\bar{p}$ production with the momentum is much weaker. No momentum dependence between 1.0 and 1.5 GeV/c is observed for Ne + Sn, ($\sigma_{inv} = 88.3(\pm 24.4)$ nb · GeV/(GeV/c)^3 and $88.3(\pm 17.0)$ nb · GeV/(GeV/c)^3, respectively) a slight decrease from 1.0 to 1.5 GeV/c for Ne + NaF ($\sigma_{inv} = 68.9(\pm 18.5)$ nb · GeV/(GeV/c)^3 and $45.2(\pm 8.4)$ nb · GeV/(GeV/c)^3, respectively) and a more pronounced decrease from 1.5 to 1.9 GeV/c for Ni + Ni ($\sigma_{inv} = 127(\pm 38)$ nb · GeV/(GeV/c)^3 and $53.5\left(\begin{smallmatrix}+24.6\\-17.7\end{smallmatrix}\right)$ nb · GeV/(GeV/c)^3, respectively).

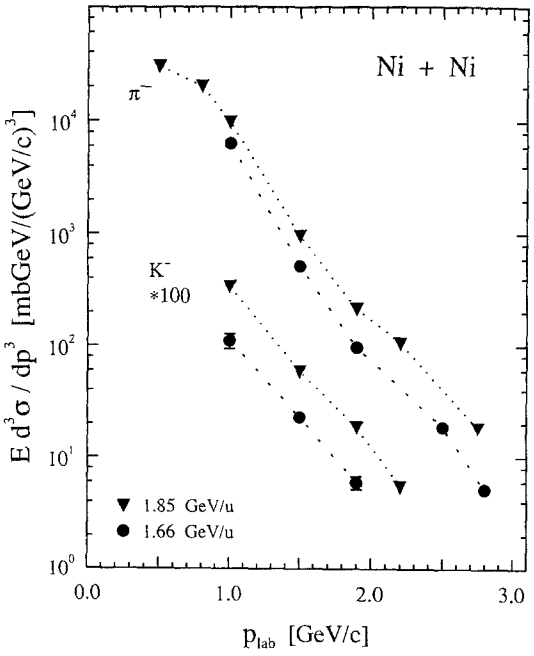

Fig. 4. K^- and π^- production cross sections measured in the collision of 1.85 GeV/u and 1.66 GeV/u ^{58}Ni with Ni as a function of the particle momentum. For better visualization the data are connected by *dotted lines* and the K^- data are scaled by a factor 100

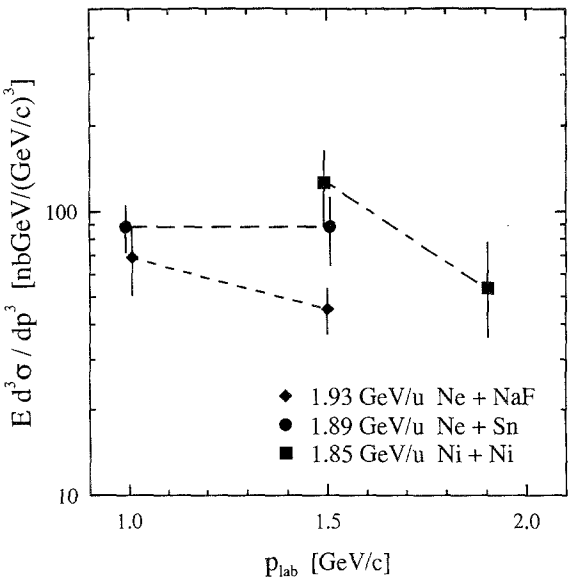

Fig. 5. Measured $\bar{p}$ production cross section in the reactions 1.93 GeV/u Ne + NaF, 1.89 GeV/u Ne + Sn and 1.85 GeV/u Ni + Ni as a function of the $\bar{p}$ momentum. The projectile energies given are mean energies in the targets

The $\bar{p}$ production cross sections measured for 1.90 GeV/u Ne + Cu and 1.87 GeV/u Ne + Bi at $p_{\bar{p}} = 1.5$ GeV/c follow the expected trend of increasing particle yield with increasing size of the colliding system, similar to the π^- and K^- cross sections. With $\sigma_{inv} = 111(\pm 19)$ nb · GeV/(GeV/c)^3 the $\bar{p}$ production cross section measured in 2 GeV/u Ne + Bi is a factor of 2.5 ± 0.6 larger than in Ne + NaF. The ratio of the $\bar{p}$ production cross sections for 1.93 GeV/u Ni + Ni and 2 GeV/u Ne + NaF is 2.8 ± 1.0, but if one takes into account the lower incident energy of the Ni beam using the measured excitation function, a higher ratio of 4.6 ± 1.6 is obtained.

The $\bar{p}$ production cross sections were also measured at lower beam energies with 1.8 GeV/u ^{20}Ne ions and 1.84 GeV/u ^{58}Ni ions, coresponding to effective incident energies of 1.69 GeV/u for Ne + Sn and 1.66 GeV/u for Ni + Ni, respectively. The 200 MeV/u reduction of the incident energy reduces the observed $\bar{p}$ yields by a factor of 2.7 ± 0.8 for Ne + Sn and by a factor of $5.6^{+2.6}_{-3.2}$ for Ni + Ni.

4. Discussion

4.1. Enhancement of the antiproton production

Despite the low rate of detected antiprotons, the $\bar{p}$ yield is much too high to be produced by single nucleon-nucleon collisions as calculated in [5]. Within this first col-

lision model, taking account of high momentum components of the internal momentum distribution of the nucleons, the $\bar{p}$ production cross section should be $\sim 0.1\ \mathrm{nb}\cdot\mathrm{GeV}/(\mathrm{GeV}/c)^3$ for 2 GeV/u $^{28}Si + Si$ collisions while an approximately 3 orders of magnitude higher $\bar{p}$ yield is observed. This is a strong evidence for a dominant role of multistep processes with the excitation of Δ and N^* resonances as intermediate steps, which contribute to the creation of $p\bar{p}$ pairs at incident energies in the region of 2 GeV/u. Since in the first collision model [5] the reabsorption effects for antiprotons produced in nucleus-nucleus collisions have not been taken into account, the disagreement between the measured $\bar{p}$ yield and the prediction of the model is even larger. For c.m. momenta between 0.2 and 1 GeV/c the elementary $p\bar{p}$ annihilation cross section ranges from approximately 200 mb to 50 mb [21]. Since an annihilation cross section of 100 mb corresponds to an absorption length of ~ 0.6 fm for normal nuclear matter density, only a small fraction of the created antiprotons leaves the reaction zone without being annihilated. Medium effects on the nucleon and $\bar{p}$ masses reducing the $p\bar{p}$ production threshold have an opposite influence on the $\bar{p}$ yield. Since only a small fraction of the baryon-baryon collisions in the nuclear medium is enough energetic to create a $p\bar{p}$ pair, the $\bar{p}$ yield is very sensitively related to the production threshold, and therefore medium effects on the nucleon and $\bar{p}$ masses should enhance the $\bar{p}$ production cross section.

4.2. Scaling behaviour of the particle production cross sections

Down to extreme subthreshold processes, the invariant production cross sections for all secondary particles (π^-, K^-, $\bar{p}$), measured in the $^{20}Ne + X$ reactions were observed to fulfill approximately a scaling relation, independent of the particle species:

$$Ed^3\sigma/dp^3 \propto \exp(-E_{\mathrm{prod}}/E_0). \tag{1}$$

For a given incident energy the cross section depends only on the energy required in the nucleon-nucleon center of mass frame to produce the particle with the measured momentum, $E_{\mathrm{prod}} = E_{\mathrm{thr}} + E_{\mathrm{kin}}^{\mathrm{cm}}$, where E_{thr} and $E_{\mathrm{kin}}^{\mathrm{cm}}$ are the threshold energy for the particle creation process and the kinetic energy of the particle in the center of mass, respectively. This behaviour was found by Shor et al. [3, 22] for $^{20}Ne + NaF$ and $^{28}Si + Si$ reactions. In the Ne + X reactions studied here, the inverse slope parameter of an exponential curve fitting the cross sections of all particle species is approximately $E_0 \approx 80$ MeV. The measured values are given in Table 2.

A comparison of the particle yields at a given c.m. momentum at different incident energies in the range from 1.6 to 2 GeV/u gives similar slope parameters with respect to the mean available energy per nucleon-nucleon collision E_{avail}^{NN}, as for the dependence on E_{prod}. This suggests a generalized scaling relation

$$Ed^3\sigma/dp^3 \propto \exp[(E_{\mathrm{avail}}^{NN} - E_{\mathrm{prod}})/E_0]. \tag{2}$$

Equation (2) indicates that the cross sections depend exponentially on the net energy deficit for the particle production in a binary collision. A variation of the mean available energy per NN collision or a variation of the required production energy by the same amount results in the same production cross section. The parameter E_0 in the scaling realtion has a twofold significance; for fixed incident energy it describes the spectral distribution of the produced particles and is thus related to the "temperature" in the collision zone, while it defines the excitation function for particle production for fixed c.m. momenta of the particles. The overall agreement of the measured cross sections with the generalized scaling relation (2) with $E_0 = 80$ MeV over 9 orders of magnitude is shown for the systems $^{20}Ne + NaF$ and $^{20}Ne + Sn$ in Fig. 6.

For symmetric systems as $^{20}Ne + NaF$ or $^{58}Ni + Ni$, the quantity E_{avail}^{NN} used in the scaling relation (2) is given by the center of mass kinetic energy in the nucleon-nucleon system. In asymmetric systems the numbers of participant projectile and target nucleons are different, and their ratio depends on the impact parameter. At given impact parameter b

$$E_{\mathrm{avail}}^{NN}(b) = 2\cdot\left(\frac{\sqrt{s}}{N_p + N_t} - m\right) \tag{3}$$

with the nucleon mass m and the numbers of participant projectile and target nucleons N_p and N_t, respectively. The number of participants is obtained from the geo-

Table 2. Measured inverse slope parameters E_0 as defined in relation (1) for different reactions. For the Ne induced reactions the invariant production cross section versus E_{prod} of all secondary particles was fitted by one exponential curve, for Ni + Ni the π^- and the K^- yields were fitted separately

System	E_{mean} [GeV/u]	E_{NN}^{avail} [GeV]	p_{lab} [GeV/c]	E_0 [MeV]
Ne + NaF	1.93	0.80	1.0, 1.5	82 ± 4
Ne + Cu	1.90	0.77	1.5	82 ± 4
Ne + Sn	1.89	0.74	1.0, 1.5	82 ± 1
Ne + Sn	1.69	0.67	1.5	78 ± 6
Ne + Sn	1.49	0.60	1.5	70 ± 5
Ne + Bi	1.87	0.71	1.5	80 ± 2
Ni + Ni	1.85	0.77	0.5–2.75	$117 \pm 5^{\pi}$ 104 ± 6^{K}
Ni + Ni	1.66	0.70	1.0–2.8	$117 \pm 6^{\pi}$ 109 ± 9^{K}

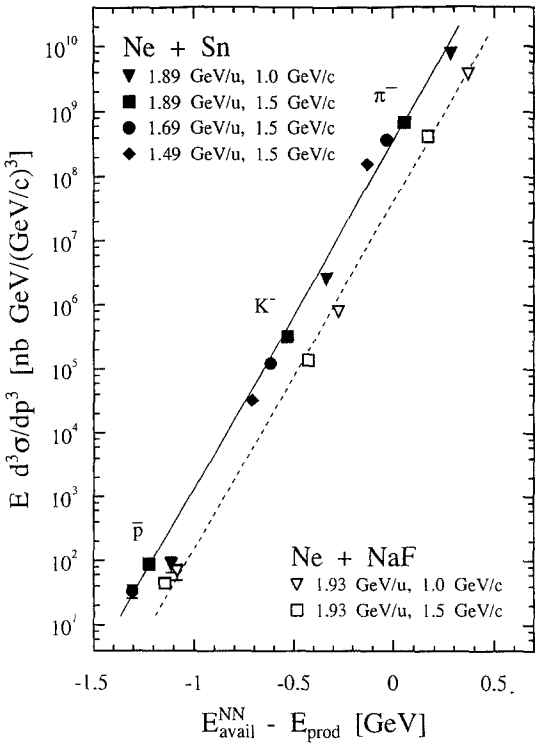

Fig. 6. Invariant production cross section for secondary particles in the reactions ^{20}Ne + NaF and ^{20}Ne + Sn as a function of the difference of the available energy per nucleon-nucleon collision and the energy required for particle production $E^{NN}_{avail} - E_{prod}$ (explanation see text). The data are roughly described by an exponential with an inverse slope $E_0 = 80$ MeV. The cross sections measured for Ne + Cu are 20% to 30% lower than for Ne + Sn, those for Ne + Bi are 20% to 30% higher

metrical overlap of projectile and target nuclei. This geometrical model is discussed in more detail in Sect. 4.4. The square of the total energy in the collision zone is

$$s = (N_p m)^2 + 2N_p(m+E)N_t m + (N_t m)^2. \quad (4)$$

For the mean available energy per NN collision we use the impact parameter averaged value

$$E^{NN}_{avail} = \frac{\int_0^{b_{max}} db\, b N^2_{part}(b)\, E^{NN}_{avail}(b)}{\int_0^{b_{max}} db\, b N^2_{part}(b)}, \quad (5)$$

which is weighted by the square of the number of participant nucleons $N_{part} = N_p + N_t$. The maximum impact parameter b_{max} is given by the sum of the nuclear radii of projectile and target $R_p + R_t$.

Secondary particles produced in the ^{58}Ni + Ni reaction were analysed within a much wider momentum range, in order to obtain π^- and K^- production cross sections in the same $E^{NN}_{avail} - E_{prod}$ regime. The maximum π^- momentum of 2.8 GeV/c corresponds to a center of mass kinetic energy of more than 1 GeV. In contrast to the scaling behaviour deduced from the data obtained in the Ne induced reactions, obviously, as can be seen in Fig. 7, in the ^{58}Ni + Ni reaction π^- and K^- cross sections are not described by a universal curve. The production cross sections for π^- are a factor 10 to 15 higher than for K^- at the same value of $E^{NN}_{avail} - E_{prod}$ in the regime where both particles were measured. A similar deviation is visible for antiprotons in Fig. 7, if one extrapolates the K^- data to low values of $E^{NN}_{avail} - E_{prod}$. A closer look at the cross sections reveals a more differentiated view on the slope parameters for the production of π^- and K^- in the various systems: from a separate fit of the π^- and K^- cross sections in the different systems one obtains inverse slope parameters $E_{0,\pi} = 116 \pm 6$ MeV and $E_{0,K} = 104 \pm 7$ MeV for ^{58}Ni + Ni, $E_{0,\pi} = 100 \pm 5$ MeV and $E_{0,K} = 89 \pm 4$ MeV for ^{20}Ne + Sn and $E_{0,\pi} = 90 \pm 3$ MeV and $E_{0,K} = 86 \pm 4$ MeV for ^{20}Ne + NaF. Comparing these values with the inverse slope parameter $E_0 \approx 80$ MeV from the generalized scaling relation (2) for all particles, the π^- and the K^- distributions deviate from a common exponential curve also in the ^{20}Ne + NaF and ^{20}Ne + Sn reactions. However these deviations are more pronounced in the ^{58}Ni + Ni reaction.

There seems to be a relation between the slope parameters and the size of the colliding system. Note that the symmetric ^{58}Ni + Ni system has on the average more participant nucleons in the collision zone than the asymmetric ^{20}Ne + Sn system (see Sect. 4.4). In a geometrical picture the spectator nucleons (more numerous in the asymmetric ^{20}Ne + Sn system), not participating in the

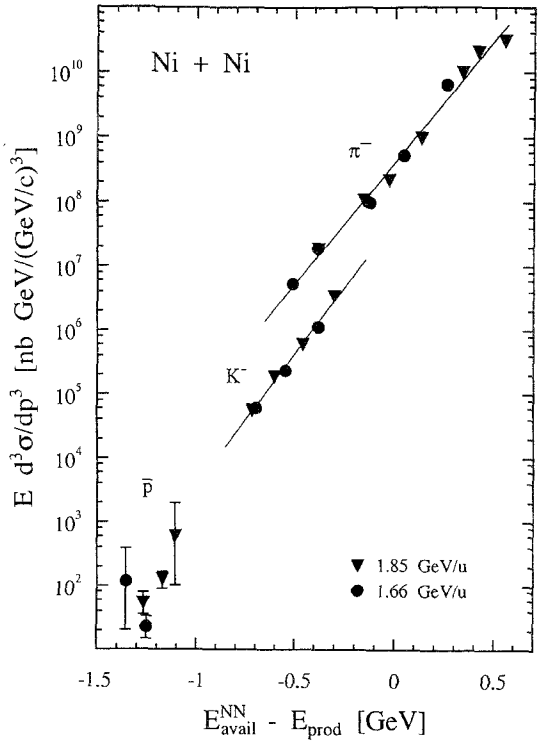

Fig. 7. Invariant production cross section for secondary particles in the relation ^{58}Ni + Ni as a function of the difference of the available energy per nucleon-nucleon collision and the energy required for particle production $E^{NN}_{avail} - E_{prod}$ (same representation as Fig. 6). The data deviate from a particle independent scaling relation. The π^- and K^- production cross sections are described by separate exponential curves with inverse slopes $E_0^{(\pi)} \approx 115$ MeV and $E_0^{(K)} \approx 105$ MeV

particle production processes, are also not relevant for the reabsorption of particles emitted at 0°. This leads to the interpretation that the different slope parameters and hence the different ratio σ_π/σ_K at the same net energy excess $(E_{\text{avail}}-E_{\text{prod}})$ is due to the increasing reabsorption probability for larger systems. Qualitatively one expects that the reabsorption probability decreases with increasing center of mass momentum. This would reduce the yield of secondary particles at low energies more than at high energies and hence shift the inverse slope of the momentum distribution towards higher values.

Experimental cross sections on π^- and K^- absorption in nuclei are available [23, 24], however nearly nothing is known about their absorption in compressed hot nuclear matter. In the medium pions are absorbed in resonances by the $\pi N \to \Delta$ channel, but the pions reappear via the decay of the Δ resonances on the surface of the collision zone or at a later state of the reaction at low densities. A fraction of the initially created pions may be lost due to the $\Delta N \to NN$ channel but in hot nuclear matter also the reverse reaction $NN \to \Delta N$ has to be considered, reducing the pion absorption probability. The K^- are absorbed by $K^- N \to (\pi) Y$ processes [8], eliminating the K^- from the observable yield. Y may be a Λ or a Σ hyperon. The larger reabsorption probability for K^- than for π^- could account for a suppression of the K^- compared to the π^- yield, i.e. for deviations from the scaling behaviour.

In this context it is interesting to compare the production cross sections of K^- mesons and of K^+ mesons, which have much lower absorption cross sections in the nuclear medium than K^- due to their antistrangeness content. Recent experiments [25] revealed that pions and K^+ mesons produced in 1.0 GeV/u Au + Au collisions have production cross sections which are well described by the scaling relation (1) with an inverse slope parameter $E_0 = 78$ MeV. This confirms the interpretation that the deviations from the scaling behaviour observed for K^- and π^- are due to reabsorption effects of K^-. It should be mentioned however that there is an inconsistency between this interpretation supported by [25, 26] and the measurement of Shor et al. [3] who observe much larger inverse slope parameters $E_0 = 240 \pm 92$ MeV for K^+ mesons in 2.0 GeV/u ^{28}Si + Si collisions.

4.3. *Excitation function of the particle production*

The slope of the excitation function is probably the most important quantity concerning subthreshold antiproton and K^- production which can be determined experimentally. Apart from minor effects due to the variation of the momentum distribution of the nucleons in the collision zone by the variation of the incident energy, the energy dependence of the $\bar{p}$ and K^- production cross section is not affected by the unknown reabsorption probability. Thus the slope of the energy dependence could yield direct information on the effective $p\bar{p}$ and K^+K^- production threshold in the hadronic medium. Due to the strong exponential dependence of the cross sections on the production energy a variation of the effective threshold by 20% as an example results in more than 2 orders of magnitude variation of the $\bar{p}$ yield.

The excitation function of particle production will be discussed in the following with respect to the available energy in the nucleon-nucleon system for fixed particle momentum in the lab system, corresponding to the experimental data. The measured cross sections are compared with the exponential relation

$$E d^3\sigma/dp^3 \propto \exp(E^{NN}_{\text{avail}}/E_x). \tag{6}$$

Note that the inverse slope parameters E_x are not identical with the slope parameters E_0 as defined in the scaling relations, because the excitation functions were measured with fixed lab momentum of the produced particles. Therefore their c.m. momenta change with changing bombarding energy. The parameter E_x is 17% ($\bar{p}$), 23% (K^-) and 25% (π^-) smaller than E_0 in the scaling relation for an energy range between 1.9 and 1.7 GeV/u.

The excitation function of $\bar{p}$ production in Ne + Sn and Ni + Ni at a $\bar{p}$ momentum of 1.5 GeV/c is shown in Fig. 8. The effective incident energies were 1.89 and 1.69 GeV/u for the ^{20}Ne + Sn reaction and 1.85 and 1.66 GeV/u for the ^{58}Ni + Ni reaction, respectively. The inverse slope parameter for the Ne + Sn system $E_x = 69 \pm 20$ MeV is in agreement with the value measured by Shor et al. [3] for ^{28}Si + Si ($E_x = 63 \pm 11$ MeV). The data suggest a steeper excitation function for

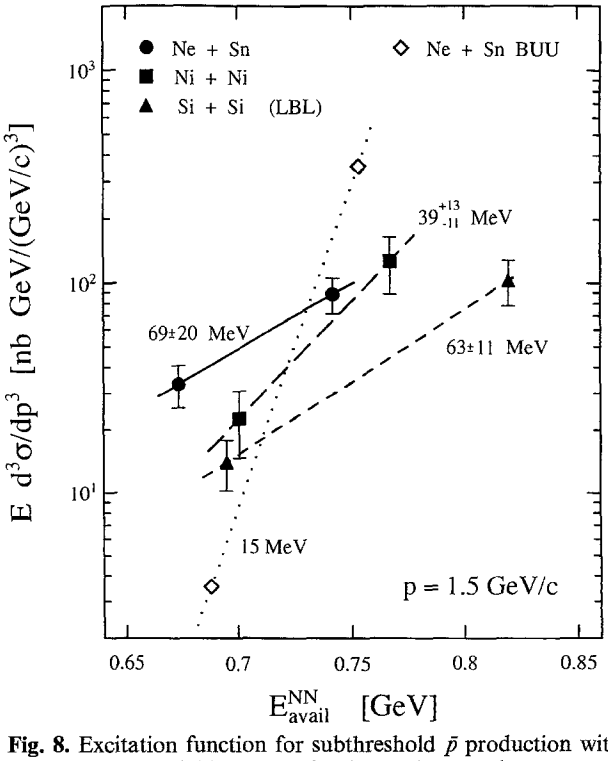

Fig. 8. Excitation function for subthreshold $\bar{p}$ production with respect to the available energy in the nucleon-nucleon system for Ne + Sn, Ni + Ni and Si + Si collisions. The Si + Si data are taken from [3]. The inverse slope parameters E_x are given for an exponential dependence on E^{NN}_{avail} as in relation (6). Using free nucleon and $\bar{p}$ masses, the calculated [33] energy dependence *(dotted line)* is much too steep

$^{58}Ni + Ni \rightarrow \bar{p} + X$ with $E_x = 39^{+13}_{-10}$ MeV, but with large statistical errors. A fit of the excitation function in the three reactions with a common slope parameter yields $E_x = 58 \pm 14$ MeV.

Similar slopes as for the $\bar{p}$ excitation function are observed for the excitation function of K^- production. For K^- with a lab momentum of 1.0, 1.5 and 1.9 GeV/c in $^{58}Ni + Ni$ inverse slope parameters E_x of 59 ± 11 MeV, 70 ± 6 MeV and 58 ± 8 MeV, respectively, were measured. In $^{20}Ne + Sn$ $E_x = 61 \pm 5$ MeV for 1.5 GeV/c K^-, resulting from the measurement at 1.49, 1.69 and 1.89 GeV/u incident energy.

For π^- production the excitation function has a larger inverse slope parameter, i.e. the π^- yield depends less on the incident energy than the yield of the heavier particles. This is particularly the case for those π^- which are produced above the threshold ($p_{lab} \leqq 1.8$ GeV/c at $E_{beam} \approx 1.8$ GeV/u): In $^{58}Ni + Ni$, $E_x = 153 \pm 25$ MeV for $p_{lab} = 1.0$ GeV/c and $E_x = 107 \pm 13$ MeV for $p_{lab} = 1.5$ GeV/c. For $p_{lab} = 1.9$ GeV/c, approximately corresponding to the threshold energy, $E_x = 83 \pm 8$ MeV. In $^{20}Ne + Sn$ $E_x = 94 \pm 6$ MeV for $p_{lab} = 1.5$ GeV/c.

As the energy required to create π^- at $p_{lab} = 1.0$ GeV/c and $p_{lab} = 1.5$ GeV/c with the corresponding c.m. energies of 0.44 GeV and 0.65 GeV, respectively, is abundantly available in NN collisions, the incident energy dependence of the process is consequently weaker than for subthreshold processes. In Fig. 9 the ratios of the particle yields for different incident energies σ (1.85 GeV/u)/σ (1.66 GeV/u) in $^{58}Ni + Ni$ and σ (1.89 GeV/u)/σ (1.69 GeV/u) in $^{20}Ne + Sn$ are presented as a function of the required production energy of the respective particle. The shaded bar in the figure indicates the available energy in the NN system at incident energies between 1.66 GeV/u and 1.85 GeV/u, and separates the region of subthreshold production on the right side from production above threshold on the left side. This ratio of the particle production cross sections increases with increasing required production energy in the region above threshold. At still higher required production energies, especially in the region below threshold this ratio seems to saturate.

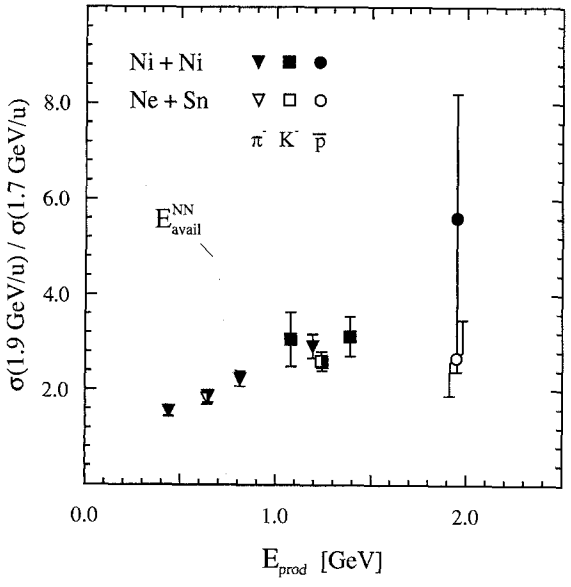

Fig. 9. Ratio of the particle yields at ~1.9 GeV/u and ~1.7 GeV/u incident energy in $^{58}Ni + Ni$ and $^{20}Ne + Sn$ as a function of the required production energy in the NN system. As this quantity varies with the incident energy, the ratios have been plotted at the mean values of E_{prod}. The ratios for π^- and for K^- at 1.5 GeV/c are almost identical for Ni + Ni and Ne + Sn. The shaded bar indicates the available energy in the NN system at incident energies between 1.66 and 1.85 GeV/u. It separates subthreshold particle production *(right)* from particle creation above the threshold *(left)*

4.4. *Influence of the system size*

In ^{20}Ne induced reactions on NaF, Cu, Sn and Bi targets the influence of the target mass on the $\bar{p}$ yield at 2 GeV/u incident energy has been studied. We observe an increase of the $\bar{p}$ production cross section with the target mass, which is less pronounced for the heavier targets.

In order to obtain a better understanding of the measured dependence of the yield on the system size, the data are compared to the prediction of a simple geometrical fireball model. Naively the size of the interaction volume as a function of the impact parameter can be estimated, if one assumes that the number of participant nucleons is given by the geometrical overlap, moving the projectile nucleus through the target nucleus. Averaging the overlap volume over the impact parameter one obtains an effective interaction volume for the different systems. This quantity is given in Table 3.

Since the $\bar{p}$ production is a subthreshold process, only a small contribution is due to single nucleon-nucleon collisions and a multistep mechanism is needed to produce the antiprotons. In the model a linear dependence on the number of $NN(N\Delta, \Delta\Delta)$ collisions and hence a quadratic dependence on the number of participants is assumed. Such a dependence is in agreement with the measurement of other particles like e.g. K^+ mesons produced below the threshold [26]. For a rough estimate of the A dependence of the $\bar{p}$ production this assumption is justified, having in mind the failure of the first collision model [5] and the dominant role of multistep processes predicted by transport theories [11]. The prediction of this geometrical fireball model for the invariant $\bar{p}$ production

Table 3. Effective sizes of the collision systems in which subthreshold antiproton production has been measured. The size is given by the number of participant nucleons which is obtained by the mean, impact parameter weighted, geometrical overlap of the projectile and the target nucleus

System	$\langle N_{part} \rangle_b$
Ne + NaF	10.2
Ne + Cu	17.5
Ne + Sn	23.3
Ne + Bi	29.9
Si + Si	13.9
Ni + Ni	29.2

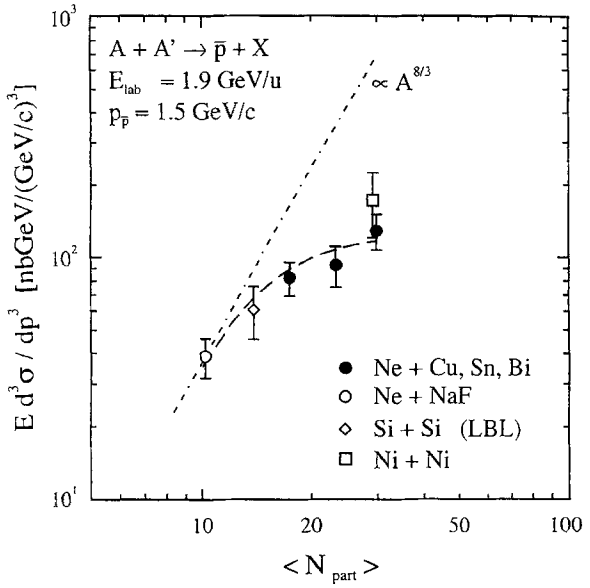

Fig. 10. Dependence of the $\bar{p}$ production cross section on the system size for symmetric and asymmetric collision systems. The mean number of participant nucleons $\langle N_{\text{part}} \rangle$ of a collision system is determined by averaging the geometrical overlap of projectile and target nuclei within the respective impact parameter range. The data for Si + Si are taken from [3]. The *dash-dotted* and *dashed curves* are predictions of the geometrical fireball model for symmetric and asymmetric systems, respectively

cross section

$$\sigma_{\text{inv}} = \sigma_0 \cdot \int_0^{b_{\max}} N_{\text{part}}^2(b) \times \exp\left[(E_{\text{avail}}^{NN}(b) - E_{\text{prod}})/E_0\right] b \, \mathrm{d}b \qquad (7)$$

with $E_0 = 70$ MeV is shown together with the $\bar{p}$ production data for Ne induced reactions in Fig. 10 as a function of the mean number of participant nucleons as given in Table 3. The dependence of the cross section on the energy difference $E_{\text{avail}}^{NN} - E_{\text{prod}}$, which is relevant for asymmetric reactions, was taken from the scaling behaviour discussed in Sect. 4.3. The slope parameter E_0 was chosen in agreement with the measured excitation function for $\bar{p}$ production in ^{20}Ne + Sn collisions. The parameter σ_0 was adjusted to the measured $\bar{p}$ yield for Ne + NaF. The small variation of the $\bar{p}$ yield for heavy targets is obtained with formula (7), since the center of mass kinetic energy has to be shared among more participant nucleons in asymmetric systems and hence E_{avail}^{NN} is smaller. The measured target mass dependence of the $\bar{p}$ yield in Ne induced reactions is well reproduced by this simple model. However, one has to consider that reabsorption effects are not included. The reabsorption probability is expected to increase quite substantially if the target mass is varied from Ne to Bi. Taking this into account, we conclude an enhancement of the primordial $\bar{p}$ production for heavy targets relative to the prediction of the geometrical model.

In asymmetric systems the observed dependence of the $\bar{p}$ yield on the system size is difficult to intepret, due to several uncertainties: apart from the unknown reabsorption probability, a considerable part of the target nucleus may not participate in the reaction, and the center of mass frame depends on the impact parameter. The influence of the system size is therefore more directly seen in the comparison of symmetric $A + A \to \bar{p} + X$ reactions, also shown in Fig. 10. The geometrical model predicts, according to (7) simply an $A^{8/3}$ dependence for the $\bar{p}$ cross section at fixed incident energy, i.e. a ratio of 16.4 for $\sigma^{\text{inv}}_{\text{Ni+Ni}\to\bar{p}+X}/\sigma^{\text{inv}}_{\text{Ne+NaF}\to\bar{p}+X}$, while the experimental ratio is only 4.6 ± 1.6. The different mean incident energies in Ne + NaF ($E_{\text{mean}} = 1.93$ GeV/u, $E_{\text{avail}}^{NN} = 0.80$ GeV) and in Ni + Ni ($E_{\text{mean}} = 1.85$ GeV/u, $E_{\text{avail}}^{NN} = 0.77$ GeV) were taken into account by a correction of the experimental $\bar{p}$ cross sections, which were scaled to the same value of E_{mean}. Due to the large statistical errors for the ^{58}Ni + Ni system, we assume that the slope of the excitation function does not depend on the system, and use $E_x = 58(\pm 14)$ MeV for the excitation function $\sigma^{\text{inv}}_{\bar{p}} \propto \exp(E_{\text{avail}}^{NN}/E_x)$ for Ne + NaF and Ni + Ni in order to compare the cross sections.

Although the geometrical picture of separated participant and spectator zones is certainly a crude simplification, the comparison of the experimental data and the model prediction indicates that the $\bar{p}$ reabsorption probability increases with the system size from Ne + NaF to Ni + Ni. Otherwise the observed dependency of the $\bar{p}$ yield on the system size is not consistent with the assumption that the probability of antiproton production per nucleus-nucleus collision increases more than linearly with the number of participant nucleons, as required for an extreme subthreshold process.

From Fig. 10 it is obvious that the experimental $\bar{p}$ data exhibit a different behaviour for symmetric and asymmetric collision systems relative to the model prediction. This may be due to the incomplete thermalization in the collision zone and thus to a significant contribution of nucleon-nucleon collisions with the full available energy in the nucleus-nucleus frame also in very asymmetric systems. We remind that the weak target mass dependence of the cross sections predicted by the model for very asymmetric systems is due to the reduction of E_{avail}^{NN}, even without reabsorption effects. Another possible explanation is a different reabsorption probability due to the different geometry in symmetric and asymmetric collision systems.

Since also the K^- are produced subthreshold one expects a similar dependence of the yield on the system size as for antiprotons. The ratio $\sigma^{\text{inv}}_{\text{Ni+Ni}\to K^-+X}/\sigma^{\text{inv}}_{\text{Ne+NaF}\to K^-+X}$ is 6.4 ± 0.4 for 1.5 GeV/c K^- and 6.4 ± 0.7 for 1.0 GeV/c K^-, respectively, within the errors not different from the ratio for antiprotons ($\sigma^{\text{inv}}_{\text{Ni+Ni}\to\bar{p}+X}/\sigma^{\text{inv}}_{\text{Ne+NaF}\to\bar{p}+X} = 4.6 \pm 1.6$). However, a weaker A dependence of the $\bar{p}$ yield than of the K^- yield, which may be due to the larger $\bar{p}$ reabsorption probability, cannot be excluded. For pions at 1.9 GeV/u incident energy the production threshold corresponds to a lab momentum of ~ 1.8 GeV/c. Pions with 1.0 and 1.5 GeV/c are therefore produced above the threshold and their production does not require multistep processes. We measure a ratio $\sigma^{\text{inv}}_{\text{Ni+Ni}\to\pi^-+X}/\sigma^{\text{inv}}_{\text{Ne+NaF}\to\pi^-+X}$ of 3.4 ± 0.2 for 1.5

GeV/c π^- and of 3.8 ± 0.3 for 1.0 GeV/c π^-, significantly lower than the ratio for K^-. This result is in agreement with the observation [26] that the yield of subthreshold particles exhibits a more pronounced A dependence than the yield of particles produced above the threshold.

4.5. *Momentum distribution*

There are two different ways to investigate the dependence of secondary particle yields on the energy available in the system relative to the required energy for their production. An approach complementary to the study of the excitation function for $\bar{p}$ production is the measurement of the $\bar{p}$ momentum distribution. Whereas the slope of the excitation function is nearly independent of the reabsorption effects, the momentum distribution is expected to be influenced by the strong decrease of the annihilation probability with increasing momentum. The momentum dependence of the $\bar{p}$ production cross section is shown in Fig. 5. For all systems the momentum dependence is rather weak, since for increasing the $\bar{p}$ momentum the effect of increasing the required energy for the production process is nearly canceled by the decreasing reabsorption probability. The small $\bar{p}$ escape probability at low center of mass momenta is not primarily due to the high elementary $\bar{p}N$ annihilation cross section (for $p_{\bar{p}} \to 0\, \sigma_{\text{ann}} \approx 200$ mb), since the nucleons in the collision zone have roughly a momentum distribution corresponding to $T \sim 80$–100 MeV, and hence $p\bar{p}$ collisions with much lower c.m. energies and corresponding annihilation cross sections of more than 100 mb are rare. This interpretation is consistent with the results of RBUU calculations [13].

The measured momenta of 1.0, 1.5 and 1.9 GeV/c correspond to kinetic energies of ~ 0, 60 and 150 MeV of the antiprotons in the center of mass system. If the scaling formula (2) with a slope parameter $E_0 \approx 80$ MeV were valid for the $\bar{p}$ momentum dependence of the cross section, i.e. $\bar{p}N$ annihilation were neglected, a decrease by a factor of ~ 2 would be expected for 1.5 GeV/c compared to 1.0 GeV/c, and a factor of ~ 3 for 1.9 GeV/c compared to 1.5 GeV/c. The observed ratios of the $\bar{p}$ cross sections, however, are considerably lower. As shown in Fig. 5, for the larger Ne + Sn system the $\bar{p}$ production cross section may even remain constant from 1.0 to 1.5 GeV/c within the experimental errors, while a slight decrease of the yield is observed for Ne + NaF. The smaller escape probability for antiprotons in the Ne + Sn reaction is evident if one compares the ratios of the $\bar{p}$ and K^- yields at 1 GeV/c for both systems:

$$\sigma^{\text{inv}}_{\text{Ne+NaF}\to\bar{p}+X} / \sigma^{\text{inv}}_{\text{Ne+NaF}\to K^-+X} = 8.5(2.3) \cdot 10^{-5}$$

and

$$\sigma^{\text{inv}}_{\text{Ne+Sn}\to\bar{p}+X} / \sigma^{\text{inv}}_{\text{Ne+Sn}\to K^-+X} = 3.5(0.9) \cdot 10^{-5}.$$

At 1.5 GeV/c the $\bar{p}/K^-$ ratios are $3.2(0.6) \cdot 10^{-4}$ for Ne + NaF and $2.7(0.5) \cdot 10^{-4}$ for Ne + Sn, i.e. they have comparable values for both systems. This reflects primarily the dependence of the $\bar{p}$ reabsorption effects on the center of mass momentum and on the system size.

The reabsorption of K^- is much less influenced by the system size, since already at 1 GeV/c kaons are well above midrapidity. At higher $\bar{p}$ momenta the variation of the reabsorption probability becomes weaker, and the momentum dependence of the observed yield is dominated by the reduced production probability. This behaviour is visible in Fig. 5 for the Ni + Ni system at 1.5 and 1.9 GeV/c. At 1.0 GeV/c in the Ni + Ni reaction only π^- and K^- were measured, the single $\bar{p}$ event observed in this run has not been included in Fig. 5. For comparison the momentum dependence is also shown for K^- and π^- in 1.66 and 1.85 GeV/u ^{58}Ni + Ni collisions in Fig. 11 in a representation in which thermal distributions appear as exponential curves. With respect to the kinetic energy in the NN system, the cross sections as a function of the kinetic energy in the NN system have inverse slopes of ~ 92 MeV for the kaons and ~ 96 MeV for the pions. Within the errors no dependence of the slopes on the incident energy is observed. These "temperature" parameters may be compared to the values of ~ 70 MeV found for K^+ and π^+ in 1 GeV/u Au + Au collisions [26], indicating that there is only a moderate increase of the temperature from 1 GeV/u to 2 GeV/u incident energy. This agrees well with the observed systematics of the "temperature" parameters in secondary particle spectra as a function of the bombarding energy [27]. Up to ~ 1 GeV/u a steep rise of the temperature parameters is found, while the increase is much weaker at higher incident energies. This behaviour is interpreted as a transformation of a major fraction of the translational kinetic energy into the excitation of the internal degrees of freedom of the nucleons, i.e. into the production of baryonic resonances, instead of a conversion into thermal energy.

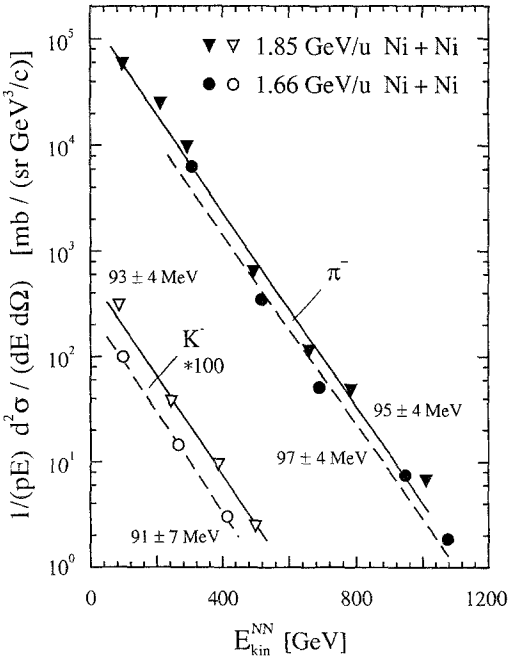

Fig. 11. Double differential cross sections for π^- and K^- production in 1.85 and 1.66 GeV/u Ni + Ni collisions as a function of the kinetic energy in the NN system. The data are compared to thermal distributions with the inverse slope parameters given in the figure. The K^- data are scaled with a factor 100

4.6. Comparison to transport models

Recently relativistic transport models were developed which take into account the quasiparticle properties of the nucleons and the antiprotons in the nuclear medium [13, 28, 29]. The reduction of the nucleon and the $\bar{p}$ masses due to medium effects result in a lower $\bar{p}$ production threshold and consequently in an enhancement of the $\bar{p}$ yield, particularly at extreme subthreshold energies. Medium effects are also taken into account for subthreshold K^- production [30]. The authors argue that without a reduction of the effective masses the calculations are not able to describe the experimental production cross sections. A different result is obtained in recent RQMD calculations for $\bar{p}$ production in 2 GeV/u Ne + NaF collisions [31], due to considerably smaller reabsorption effects in this model than in [13, 29].

In the RBUU calculations of [13] the $\bar{p}$ selfenergy in the medium was treated as a free parameter, since the real part of the potential is expected to be strongly influenced by the annihilation channel, i.e. the imaginary part of the potential. From comparison with experimental $\bar{p}$ production cross sections for Si + Si [3] and for Ni + Ni, measured by our group [32], Teis et al. [13] deduce a $\bar{p}$ selfenergy in the nuclear medium of ~ 150 MeV. The extraction of this value, however, is based on the correct treatment of the $\bar{p}$ reabsorption, which reduces the $\bar{p}$ yield by more than two orders of magnitude in this calculation.

In very recent papers Li et al. studied antiproton [29] and antikaon production [30] in a VUU model with selfenergies of the $\bar{p}$ and K^- in the medium obtained in a mean field approximation using a G-parity transformation. In both reactions attractive scalar potentials lower the effective $\bar{p}$ and K^- thresholds and thus enhance the production cross sections at low bombarding energies. A comparison to the $\bar{p}$ and K^- production cross sections measured in 1.85 GeV/u Ni + Ni collisions demonstrates that in these calculations [29, 30] in-medium mass reductions are needed both for antiprotons and K^- mesons in order to reproduce the experimental data.

Due to the insensitivity of the excitation function for $\bar{p}$ production to the unknown reabsorption effects, it is interesting to compare the measured slope parameters with the values obtained in the transport models. As shown in Fig. 8, a much steeper excitation function than measured with an inverse slope parameter $E_x \approx 15$ MeV is predicted by a BUU calculation [33] for Ne + Sn. It includes $\bar{p}$ production via ΔN and $\Delta\Delta$ collisions (which are the dominant channels) and uses the free nucleon and antiproton masses, and does not take into account reabsorption effects. The much higher observed $\bar{p}$ yield at low incident energies indicates that the $\bar{p}$ production threshold is reduced in the nuclear medium compared to the free threshold. With the recent RBUU calculations [13] much better agreement is obtained also for the slope of the excitation function. For the reaction Ni + Ni $\rightarrow \bar{p} + X$ the excitation function of the $\bar{p}$ production was calculated for incident energies from 1.4 to 2.5 GeV/u, using an attractive $\bar{p}$ potential of -100 MeV. Between 1.6 and 1.85 GeV/u an inverse slope parameter of 68 MeV with respect to the available energy in the NN system is obtained in these calculations, which should be compared with the value 39^{+13}_{-10} MeV obtained for Ni + Ni experimentally.

5. Summary and outlook

Antiproton production in Ne + NaF, Cu, Sn and Bi and in Ni + Ni collisions has been investigated at far subthreshold energies. Simultaneously to the $\bar{p}$ production the π^- and K^- yield at 0° was measured. The previously [3] observed scaling of secondary particle yields with respect to the energy and the mass of the particles was extended to the dependence on the bombarding energy. The scaling behaviour has been confirmed in the Ne induced reactions with $p = 1.0$ and 1.5 GeV/c, i.e. within a similar limited range of particle momenta. In Ni + Ni collisions π^- and K^- cross sections, measured in a much wider momentum range, however, are not described by a single exponential curve. A gap between the π^- and the K^- yield for the same value of E_{prod} may result from K^- absorption effects, but it is questionable whether the scaling really holds over this wide range of momenta for each particle species in the other systems studied so far, and how large the influence of the system size on the deviations is.

The excitation function for $\bar{p}$ production is much flatter than theoretically predicted, if the free nucleon and antiproton masses are used, even if multistep processes (e.g. ΔN, $\Delta\Delta$ collisions) are included. It has been demonstrated [13] that flatter excitation functions are obtained if medium effects on the masses are taken into account. In a direct comparison of calculated $\bar{p}$ production cross sections with experimental data the $\bar{p}$ yield measured in Ni + Ni collisions has been used [13, 28] to deduce the $\bar{p}$ selfenergy in the hadronic medium. The consistency, however, is based on the correct prediction of the reabsorption probability. More reliable conclusions on the $\bar{p}$ selfenergy may be obtained from a comparison of the calculated and the measured slope of the excitation function, which is almost independent of the reabsorption.

In order to interpret the dependence of the $\bar{p}$ yield on the system size, the experimental data were compared to the prediction of a simple geometrical fireball model. In this model the $\bar{p}$ yield per nucleus-nucleus collision has a quadratic dependence on the number of participant nucleous. The $\bar{p}$ production cross section measured in symmetric reactions shows a weaker increase with the system size than predicted by the model, which indicates an increasing reabsorption probability for heavier systems. The target mass dependence in asymmetric systems, which is in agreement with the model prediction neglecting reabsorption effects, is more difficult to interpret.

A very weak momentum dependence of the $\bar{p}$ yield is observed for $p_{\text{lab}} < 1.5$ GeV/c, i.e. low center of mass momenta $p_{\text{c.m.}} < 0.3$ GeV/c, due to the decreasing absorption probability with the increasing escape velocity of the antiprotons. At 1 GeV/c the influence of the system size on the $\bar{p}$ reabsorption probability is clearly visible.

From the momentum distribution of the K^- and π^- "temperature" parameters of ~ 92 MeV and ~ 96 MeV respectively are derived. This parameter shows whithin the error no dependence on the incident energy between 1.66 and 1.85 GeV/u, which is consistent with the interpretation that at incident energies in the region of 2 GeV/u additional translational kinetic energy is mainly absorbed via the excitation of baryonic resonances.

In forthcoming experiments it is planned to extend the measurement of the subthreshold $\bar{p}$ and K^- production to lower incident energies in Ne + NaF and Ni + Ni, and to determine the slope of the excitation function to a better accuracy. On the other hand also measurements at high $\bar{p}$ momenta up to 2.7 GeV/c are foreseen. At the corresponding center of mass kinetic energies up to ~ 0.4 GeV, significantly above typical thermal energies of ~ 100 MeV, the $\bar{p}$ escape probability is expected to increase considerably.

On the theoretical side, further investigation of the influence of the nuclear medium on the excitation function will deepen our understanding of $\bar{p}$ and K^- production at far subthreshold energies. More comprehensive calculations including also the π^- and the K^- production under identical experimental conditions will certainly be helpful.

The authors acknowledge the support of the FRS group, especially of G. Münzenberg, K. Sümmerer, K.H. Behr, A. Brünle and K.H. Burkhard. The authors also express their thanks to W. Cassing, T. Maruyama, U. Mosel and S. Teis, A. Jahns, C. Spieles and H. Stöcker, and H.H. Wolter for fruitful discussions.

References

1. Cassing, W., Metag, V., Mosel, U., Niita, K.: Phys. Rep. **188**, 363 (1990)
2. Mosel, U.: Annu. Rev. Nucl. Part. Sci. **41**, 29 (1991)
3. Shor, A., et al.: Phys. Rev. Lett. **63**, 2192 (1989)
4. Baldin, A.A., et al.: JETP Lett. **47**, 137 (1988)
5. Shor, A., Perez-Mendez, V., Ganezer, K.: Nucl. Phys. A**514**, 717 (1990)
6. Dorfan, D.E., et al.: Phys. Rev. Lett. **14**, 995 (1965)
7. Danielewicz, P.: Phys. Rev. C**42**, 1564 (1990)
8. Koch, P., Dover, C.B.: Phys. Rev. C**40**, 145 (1989)
9. Ko, C.M., Ge, X.: Phys. Lett. B**205**, 195 (1988); Ko, C.M., Xia, L.H.: Phys. Rev. C**40**, R1118 (1989)
10. Lang, A., Blättel, B., Koch, V., Weber, K., Cassing, W., Mosel, U.: Phys. Lett. B**245**, 147 (1990)
11. Batko, G., Cassing, W., Mosel, U., Niita, K., Wolf, Gy.: Phys. Lett. B**256**, 331 (1991)
12. Huang, S.W., Li, G.Q., Maruyama, T., Faessler, A.: Nucl. Phys. A**547**, 653 (1992)
13. Teis, S., Cassing, W., Maruyama, T., Mosel, U.: Phys. Lett. B**319**, 47 (1993); Teis, S., Cassing, W., Maruyama, T., Mosel, U.: (submitted to Phys. Rev. C)
14. Ahner, W., et al.: Z. Phys. A**341**, 123 (1991)
15. Berg, F.D., et al.: Z. Phys. A**337**, 351 (1990)
16. Walcher, T.: Annu. Rev. Nucl. Part. Sci. **38**, 67 (1989)
17. Amsler, C.: Annu. Rev. Nucl. Part. Sci. **41**, 219 (1991)
18. Geissel, H., et al.: Nucl. Instrum. Methods B**70**, 286 (1992)
19. Schröter, A., Koenig, W., Berdermann, E., Kienle, P., Ströher, H., Homolka, J., Schumacher, F.: GSI Scientific Report 91-1, 293 (1991); Schröter, A.: GSI Report 93-33, 1 (1993)
20. Ziegler, C., Brohm, T., Clerc, H.-G., Geissel, H., Schmidt, K.-H., Sümmerer, K., Vieira, D.J., Voss, B.: GSI Scientific Report 91-1, 291 (1991)
21. Flaminio, V., Moorhead, W.G., Morrison, D.R.O., Rivoire, N.: CERN-HERA Report 84-01, 147 (1984)
22. Shor, A.: Phys. Lett. B**274**, 11 (1992)
23. Nakai, N., Kobayashi, T., Numao, T., Shibata, T.A., Chiba, J., Masutani, K.: Phys. Rev. Lett. **44**, 1446 (1980)
24. Afonas'ev, V.N., et al.: Sov. J. Nucl. Phys. **47**, 1049 (1988)
25. Grosse, E.: Private communication (1992)
26. Senger, P., et al.: Nucl. Phys. A**553**, 757c (1993); Miśkowiec, D., et al.: (to be published in Phys. Rev. Lett.), Preprint GSI-94-28
27. Metag, V.: Nucl. Phys. A**553**, 283c (1993)
28. Batko, G., Faessler, A., Huang, S.W., Lehmann, E., Puri, R.K.: (to be published in J. Phys. G)
29. Li, G.Q., Ko, C.M., Fang, X.S., Zheng, Y.M.: Phys. Rev. C**49**, 1139 (1994); Li, G.Q., Ko, C.M.: (submitted to Phys. Rev. Lett.)
30. Li, G.Q., Ko, C.M., Fang, X.S.: (to be published in Phys. Rev. C)
31. Spieles, C., Jahns, A., Sorge, H., Stöcker, H., Greiner, W.: Mod. Phys. Lett. A**8**, 27 (1993)
32. Schröter, A., et al.: Nucl. Phys. A**553**, 775c (1992); Gillitzer, A., et al.: Proc. XXXI Int. Winter Meeting on Nucl. Phys., Bormio 1993, p. 546
33. Cassing, W., Teis, S.: Private communication (1992)